Inorg. Chem. **2005**, *44*, 4737−4746

Syntheses and Properties of Emissive Iridium(III) Complexes with Tridentate Benzimidazole Derivatives

Tomona Yutaka,[†] Shinya Obara,[†] Satoshi Ogawa,[†] Koichi Nozaki,[‡] Noriaki Ikeda,[‡] Takeshi Ohno,[‡] Youichi Ishii,[†] Ken Sakai,[§] and Masa-aki Haga*,[†]

Department of Applied Chemistry, Faculty of Science and Engineering, Chuo University, 1-13-27 Kasuga, Bunkyo-ku, Tokyo 112−8551, Japan, Department of Chemistry, Graduate School of Science, Osaka University, 1-16 Machikaneyama, Toyonaka, Osaka 560-0043, Japan, and Department of Chemistry, Graduate School of Science, Kyushu University, 6-10-1 Hakozaki, Higashi-ku, Fukuoka 812-8581, Japan

Received October 2, 2004

A series of novel emissive Ir(III) complexes having the coordination environments of $[Ir(N\wedge N\wedge N)_2]^{3+}$, $[Ir(N\wedge N\wedge N)(N\wedge N)Cl]^{2+}$, and $[Ir(N\wedge N\wedge N)(N\wedge C\wedge N)]^{2+}$ with 2,6-bis(1-methyl-benzimidazol-2-yl)pyridine (**L1**, N∧N∧N), 1,3-bis(1-methyl-benzimidazol-2-yl)benzene (**L2H**, N∧C∧N), 4′-(4-methylphenyl)-2,2′:6′,2″-terpyridine (ttpy, N∧N∧N), and 2,2′-bipyridine (bpy, N∧N) have been synthesized and their photophysical and electrochemical properties studied. The Ir(III) complexes exhibited phosphorescent emissions in the 500–600 nm region, with lifetimes ranging from approximately 1–10 μs at 295 K. Analysis of the 0–0 energies and the redox potentials indicated that the lowest excited state of $[Ir(\mathbf{L1})(\mathbf{L2})]^{2+}$ possessed the highest contribution of ^{3}MLCT (MLCT = metal-to-ligand charge transfer) among the Ir(III) complexes, reflecting the σ-donating ability of the tridentate ligand, ttpy < **L1** < **L2**. The emission quantum yields (Φ) of the Ir(III) complexes ranged from 0.037 to 0.19, and the highest Φ value (0.19) was obtained for $[Ir(\mathbf{L1})(bpy)Cl]^{2+}$. Radiative rate constants (k_r) were 1.2×10^4 s^{-1} for $[Ir(ttpy)_2]^{3+}$, 3.7×10^4 s^{-1} for $[Ir(\mathbf{L1})(bpy)Cl]^{2+}$, 3.8×10^4 s^{-1} for $[Ir(ttpy)(bpy)Cl]^{2+}$, 3.9×10^4 s^{-1} for $[Ir(\mathbf{L1})_2]^{3+}$, and 6.6×10^4 s^{-1} for $[Ir(\mathbf{L1})(\mathbf{L2})]^{2+}$. The highest radiative rate for $[Ir(\mathbf{L1})(\mathbf{L2})]^{2+}$ with the highest contribution of ^{3}MLCT could be explained in terms of the singlet–triplet mixing induced by spin–orbit coupling of 5d electrons in the MLCT electronic configurations.

Introduction

The photochemical and photophysical properties of d^6 or d^8 transition-metal complexes such as Ru(II),[1] Re(I),[2] and Pt(II)[3] have been studied extensively because of their characteristic emission properties and their applications in areas such as energy conversion, organic LEDs, luminescent sensors, and so forth. As for the coordination environment around the metal ion, the majority of complexes are primarily surrounded by pyridyl nitrogens. In addition, other cases such as metal−sulfur and metal−carbon bonds have been reported in the literature.[3a] Recently, Ir(III) complexes have been the subject of much study with regard to their application as emitters in electroluminescence (EL) devices.[4] Because Ir(ppy)$_3$ (ppy^- = 2-phenylpyridine anion) and its derivatives have been extensively examined because of their high emission quantum yields, cyclometalated Ir(III) complexes have been recognized as potential candidates for application

* To whom correspondence should be addressed. E-mail: mhaga@chem.chuo-u.ac.jp.
[†] Chuo University.
[‡] Osaka University.
[§] Kyushu University.

(1) (a) Balzani, V.; Campagna, S.; Denti, G.; Juris, A.; Serroni, S.; Venturi, M. *Coord. Chem. Rev.* **1994**, *132*, 1−13. (b) Flamigni, L.; Encinas, S.; Barigelletti, F.; MacDonnell, F. M.; Kim, K.-J.; Puntoriero, F.; Campagna, S. *J. Chem. Soc., Chem. Commun.* **2000**, 1185−1186. (c) Balzani, B.; Juris, A. *Coord. Chem. Rev.* **2001**, *211*, 97−115. (d) Welter, S.; Brunner, K.; Hofstraat, J. W.; De Cola, L. *Nature* **2003**, *421*, 54−57. (e) Fan, F.-R. F.; Bard, A. J. *J. Phys. Chem. B* **2003**, *107*, 1781−1787. (f) Duati, M.; Tasca, S.; Lynch, F. C.; Bohlen, H.; Vos, J. G.; Stagni, S.; Ward, M. D. *Inorg. Chem.* **2003**, *42*, 8377−8384. (g) Liu, F.; Wang, K.; Bai, G.; Zhang, Y.; Gao, L. *Inorg. Chem.* **2004**, *43*, 1799−1806.

(2) (a) Stufkens, D. J.; Aarnts, M. P.; Rossenaar, B. D.; Vlcek, A. *Coord. Chem. Rev.* **1998**, *177*, 127−179. (b) Yam, V. W.-W.; Yang, Y.; Zhang, J.; Chu, B. W.-K.; Zhu, N. *Organometallics* **2001**, *20*, 4911−4918. (c) Lo, K. K.-W.; Hui, W.-K.; Ng, D. C.-M.; Cheung, K.-K. *Inorg. Chem.* **2003**, *41*, 40−46. (d) Ranjan, S.; Lin, S.-Y.; Hwang, K.-C.; Chi, Y.; Ching, W.-L.; Liu, C.-S.; Tao, Y.-T.; Chien, C.-H.; Peng, S.-M.; Lee, G.-H. *Inorg. Chem.* **2003**, *42*, 1248−1255. (e) Rajendran, T.; Manimaran, B.; Liao, R.-T.; Lin, R.-J.; Thanasekaran, P.; Lee, G.-H.; Peng, S.-M.; Liu, Y.-H.; Chang, I. -J.; Rajagopal, S.; Lu, K.-L. *Inorg. Chem.* **2003**, *42*, 6388−6394. (f) Wong, K. M.-C.; Lam, S. C.-F.; Ko, C.-C.; Zhu, N.; Yam. V. W.-W.; Roue, S.; Lapinte, C.; Fathallah, S.; Costuas, K.; Kahlal, S.; Halet, J.-F. *Inorg. Chem.* **2003**, *42*, 7086−7097.

10.1021/ic048622z CCC: $30.25
Published on Web 05/26/2005

in EL devices.[4] Compared to the metal−N bond, anionic C coordination leads to a higher ligand field strength. Although there are many Ir(III) complexes with bidentate ligands, only limited examples of Ir(III) complexes with tridentate ligands are known.[4b,h−j,l]

We have studied the redox and photochemical properties of Ru(II) and Pt(II) complexes with tridentate 2,6-bis(benzimidazolyl-2-yl)pyridine ligand and its derivatives.[5] Compared to tridentate terpyridine (tpy), 2,6-bis(benzimidazolyl-2-yl)pyridine acts as a moderate σ donor and also as a π acceptor. The substitution of N heteroatoms with carbon atoms in these tridentate ligands results in a tuning of the photochemical properties of Ir(III) complexes. 2,6-Bis(phenyl)pyridine, in which two ancillary pyridine groups in terpyridine are replaced by phenyl groups, has been reported to be coordinated to an Ir(III) center as a C∧N∧C tridentate ligand.[4i] Several studies of the photophysical properties of Ru(II) and Pt(II) complexes with cyclometallating tridentate ligands have been reported.[6] In particular, Pt(II) complexes with 1,3-di-(2-pyridyl)benzene derivatives have been found to exhibit higher emission quantum yields (0.58−0.68).[6e]

In the present paper, 1,3-bis(benzimidazolyl-2-yl)benzene was employed as a tridentate ligand including an Ir−C σ bond, which plays an important role in strengthening the ligand field and increasing the emission quantum yield of the complex. We synthesized a series of novel Ir(III) complexes with 2,6-bis(1-methyl-benzimidazol-2-yl)pyridine (**L1**) and 1,3-bis(1-methyl-benzimidazol-2-yl)benzene (**L2H**) as tridentate ligands, as shown in Chart 1. The effects of the coordination environment in $[Ir(N∧N∧N)_2]^{3+}$, $[Ir(N∧N∧N)(N∧N)Cl]^{2+}$, and $[Ir(N∧N∧N)(N∧C∧N)]^{2+}$ for $[Ir(\mathbf{L1})_2]^{3+}$, $[Ir(\mathbf{L1})(bpy)Cl]^{2+}$, and $[Ir(\mathbf{L1})(\mathbf{L2})]^{2+}$, respectively, on photophysical properties have been examined, where the notations N∧N∧N, N∧C∧N, and N∧N indicate the coordinated atoms in the ligands and **L1**, **L2**, and **L2H** are the abbreviations for the ligands.

Chart 1

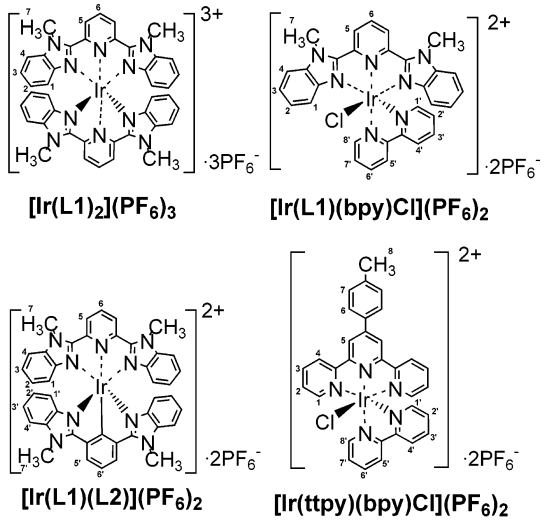

Experimental Section

Materials. $Zn(NO_3)_2·6H_2O$ (Wako), NH_4PF_6 (Wako), isophthalic acid (Aldrich), *N*-methyl-1,2-phenylenediamine (Aldrich), 4′-(4-methylphenyl)-2,2′:6′,2″-terpyridine (ttpy) (Aldrich), and $IrCl_3·nH_2O$ (Soekawa) were used as received. The other synthetic reagents were purchased from Kanto Kagaku and used as received. For the photophysical measurements, acetonitrile, *N*,*N*-dimethylformamide (spectroscopic grade), methanol, and ethanol (HPLC grade) were purchased from Kanto Kagaku and used as received. For the electrochemical measurements, acetonitrile was distilled over P_2O_5, and tetra-*n*-butylammonium tetrafluoroborate (Nacalai) was purified by recrystallization from EtOH. 4′-Tolyl-2,2′:6′,2″-terpyridine iridium trichloride ($Ir(ttpy)Cl_3$)[4b] and 2,6-bis(1-methyl-benzimidazol-2-yl)pyridine ligand (**L1**)[7] were prepared according to the literature.

Physical Measurements. ^{1}H NMR, ESI−MS, MALDI-TOF−MS, and UV−vis spectra were recorded with a Mercury 300 (Varian) or JNM-ECA 500 (JEOL) spectrometer, a Micromass LCT mass spectrometer, a Shimadzu AXIMA-CFR, and a Hewlett-Packard 8453 UV−vis spectrophotometer, respectively. For the assignment of ^{1}H NMR spectra, the proton numbering system in Chart 1 is used in this paper. Electrochemical measurements were carried out in a standard one-compartment cell under N_2 gas, equipped with a BAS platinum (ϕ 1.6 mm) or a BAS glassy-carbon (ϕ 3 mm) working electrode, a platinum wire counter electrode,

(3) (a) Hissler, M.; McGarrah, J. E.; Connick, W. B.; Geiger, D. K.; Cummings, S. D.; Eisenberg, R. *Coord. Chem. Rev.* **2000**, *208*, 115−137. (b) Michalec, J. F.; Bejune, S. A.; Cuttell, D. G.; Summerton, G. C.; Gertenbach, J. A.; Field, J. S.; Haines, R. J.; McMillin, D. R. *Inorg. Chem.* **2001**, *40*, 2193−2200. (c) Yam, V. W.-W.; Tang, R. P.-L.; Wong, K. M.-C.; Lu, X-X.; Cheung, K.-K.; Zhu, N. *Chem.—Eur. J.* **2002**, *8*, 4066−4076. (d) Williams, J. A. G.; Beeby, A.; Davies, E. S.; Weinstein, J. A.; Wilson, C. *Inorg. Chem.* **2003**, *42*, 8609−8611. (e) Yam, V. W.-W.; Wong, K. M.-C.; Zhu, N. *Angew. Chem., Int. Ed.* **2003**, *42*, 1400−1403. (f) Che, C.-M.; Fu, W.-F.; Lai, S.-W.; Hou, Y.-J.; Liu, Y.-L. *J. Chem. Soc., Chem. Commun.* **2003**, 118−119.

(4) (a) Maestri, M.; Balzani, V.; Deuschel-Cornioley, C.; von Zelewsky, A. *Adv. Photochem.* **1992**, *17*, 1−78. (b) Collin, J.-P.; Dixon, I. M.; Sauvage, J.-P.; Williams, J. A. G.; Barigelletti, F.; Flamigni, L. *J. Am. Chem. Soc.* **1999**, *121*, 5009−5016. (c) Lamansky, S.; Djurovich, P.; Murphy, D.; Adbel-Razzaq, F.; Lee, H.-E.; Adachi, C.; Burrows, P. E.; Forrest, S. R.; Thompson, M. E. *J. Am. Chem. Soc.* **2001**, *123*, 4304−4312. (d) Nazeeruddin, M. K.; Humphry-Baker, R.; Berner, D.; Rivier, S.; Zuppiroli, L.; Graetzel, M. *J. Am. Chem. Soc.* **2003**, *125*, 8790−8797. (e) Plummer, E. A.; Hofstraat, J. W.; De Cola, L. *J. Chem. Soc., Dalton Trans.* **2003**, 2080−2084. (f) Tsuboyama, A.; Iwasaki, H.; Furugori, M.; Mukaide, T.; Kamatani, J.; Igawa, S.; Moriyama, T.; Miura, S.; Takiguchi, T.; Okada, S.; Hoshino, M.; Ueno, K. *J. Am. Chem. Soc.* **2003**, *125*, 12971−12979. (g) Lo, K. K.-M.; Chung, C.-K.; Lee, T. K.-M.; Lui, L.-H.; Tsang, K. H.-K.; Zhu, N. *Inorg. Chem.* **2003**, *42*, 6886−6897. (h) Yoshikawa, N.; Matsumura-Inoue, T. *Anal. Sci.* **2003**, *19*, 761−765. (i) Polson, M.; Fracasso, S.; Bertolasi, V.; Ravaglia, M.; Scandola, F. *Inorg. Chem.* **2004**, *43*, 1950−1956. (j) Baranoff, E.; Dixon, I. M.; Collin, J.-P.; Sauvage, J.-P.; Ventura, B.; Flamigni, L. *Inorg. Chem.* **2004**, *43*, 3057−3066. (k) Huang, W.-S.; Lin, J. T.; Chien, C.-H.; Tao, Y.-T.; Sun, A.-S.; Wen, Y.-S. *Chem. Mater.* **2004**, *16*, 2480−2488. (l) Leslie, W.; Batsanov, A. S.; Howard, J. A. K.; Williams, J. A. G. *J. Chem. Soc., Dalton Trans.* **2004**, 623.

(5) (a) Xiaoming, X.; Haga, M.; Matsumura-Inoue, T.; Ru, Y.; Addison, A. W.; Kano, K. *J. Chem. Soc., Dalton Trans.* **1993**, 2477−2484. (b) Wang, K.; Haga, M.; Monjushiro, H.; Akiba, M.; Sasaki, Y. *Inorg. Chem.* **2000**, *39*, 4022−4028. (c) Haga, M.; Hong, H.-G.; Shiozawa, Y.; Kawata, Y.; Monjushiro, H.; Fukuo, T.; Arakawa, R. *Inorg. Chem.* **2000**, *39*, 4566−4573.

(6) (a) Chung, T.-C.; Cheung, K.-K.; Peng, S.-M.; Che, C.-M. *J. Chem. Soc., Dalton Trans.* **1996**, 1645−1651. (b) Lai, S.-W.; Chan, M. C.-W.; Cheung, T. C.; Peng, S.-M.; Che, C.-M *Inorg. Chem.* **1999**, *38*, 4046−4055. (c) Barigelletti, F.; Ventura, B.; Collin, J.-P.; Kayhanian, R.; Gaviña, P.; Sauvage, J.-P. *Eur. J. Inorg. Chem.* **2000**, 113−119. (d) Bonnefous, C.; Chouai, A.; Thummel, R. *Inorg. Chem.* **2001**, *40*, 5851−5859. (e) Williams, J. A. G.; Beeby, A.; Dabies, E. S.; Weinstein, J. A.; Wilson, C. *Inorg. Chem.* **2003**, *42*, 8609−8611.

(7) Addison, A. W.; Burke, P. J. *J. Heterocycl. Chem.* **1981**, *18*, 803−805.

Table 1. Crystal Data and Structure Refinement for Ir(III) Complexes

	$[Ir(\mathbf{L1})_2](PF_6)_3 \cdot 3CH_3CN$	$[Ir(\mathbf{L1})(bpy)Cl](PF_6)_2 \cdot 2CH_3CN$	$[Ir(\mathbf{L1})(\mathbf{L2})](BPh_4)_2 \cdot CH_3CN$
empirical formula	$C_{48}H_{43}IrN_{13}P_3F_{18}$	$C_{37}H_{34}IrN_{10}ClP_2F_{12}$	$C_{93}H_{77}IrN_{10}B_2$
fw	1429.06	1136.34	1548.54
cryst color, habit	reddish orange, prism	orange, prism	brown, prism
cryst dimensions	0.19 × 0.16 × 0.15 mm	0.30 × 0.30 × 0.15 mm	0.80 × 0.70 × 0.30 mm
cryst syst	monoclinic	monoclinic	monoclinic
a (Å)	15.2218(12)	11.493(4)	17.204(5)
b (Å)	19.3547(16)	17.003(5)	20.227(6)
c (Å)	18.8514(15)	21.177(6)	21.092(6)
β (deg)	91.368(2)	102.756(5)	94.187(4)
V (Å^3)	5552.3(8)	4036.2(21)	7319.6(34)
space group	$P2_1/n$	$P2_1/n$	$P2_1/n$
Z	4	4	4
D_{calc} (g/cm^3)	1.710	1.802	1.405
F_{000}	2824	2144	3168
$R_1{}^a$ [$I > 2.00\sigma(I)$]	0.0343	0.045	0.036
$wR_2{}^b$	0.0967	0.086	0.112
GOF^c	1.023	1.026	1.011

[a] $R_1 = \Sigma||F_o| - |F_c||/|F_o|$. [b] $wR_2 = [\Sigma w(|F_o|^2 - |F_c|^2)^2/\Sigma w(|F_o|^2)^2]^{1/2}$. [c] GOF $= [\Sigma w(|F_o|^2 - |F_c|^2/(N_o - N_V)]^{1/2}$, where N_o = number of observations and N_V = number of variables.

and a Ag/Ag^+ reference electrode with an ALS/CH model 660A electrochemical analyzer. The reference electrode was $Ag/AgNO_3$ (0.01 M in 0.1 M $TBABF_4$ CH_3CN), abbreviated as Ag/Ag^+. The ferrocene/ferrocenium (Fc/Fc^+) oxidation process was used as an internal reference standard, and all potentials are reported versus Fc/Fc^+. The $E_{1/2}$ values for the Fc/Fc^+ couple were +0.04 V versus Ag/Ag^+, which was found to be 0.33 V more negative than that versus SCE. Emission spectra were recorded using a grating monochromator (Triax 1900, Jobin Yvon) with a CCD image sensor (S7031, Hamamatsu). The spectral sensitivity of the spectrofluorometer was corrected using a bromine lamp (IPD 100V 500WCS, Ushio). A sample solution in a 1-mm quartz cell was deoxygenated and excited using an LD-excited solid-state Nd:YAG laser (355 nm, 440 ps, 13 kHz, 6 mW, JDS Uniphase). For the measurement of phosphorescence from the Zn(II) compound, the fluorescence component was blocked using a rotating sector. The emission quantum yields of the Ir(III) compounds were determined using 9,10-diphenylanthracene (DPA; $\phi = 0.91$) as a reference.[8] Depolarized light was used in all cases for determination of the emission quantum yield. For the determination of electron-vibration coupling constants or Huang−Rhys factors of accepting modes, a one-mode Franck−Condon analysis of emission spectra was used.[9] Eq 1 in ref 10b was used for the determination of Haung-Rhys (S) factors from a single-mode Franck−Condon analysis of emission spectra.

For the determination of emission lifetimes, the deoxygenated sample solution was photoexcited using the pulsed Nd:YAG laser. The light from the sample was monochromated using a grating monochromator (H-20, Jobin Yvon) and converted into current signals by a photomultiplier tube (R3896, Hamamatsu). The transient signals for 2560−10240 shots were accumulated on a digitizing oscilloscope (HP 54 520 Hewlett-Packard) to get the decay profile of the emission intensity, which was fit to two or three exponential functions with convolution of the instrumental response function of the measuring system. The time resolution of the system was 2 ns. The measurements at 77 K were performed using a cylindrical quartz cell (1 mm inner diameter) and a liquid-nitrogen dewar.

Crystal Structure Determination. Diffraction data of $[Ir(\mathbf{L1})_2](PF_6)_3$ at 296 K were collected on a Bruker Smart APEX CCD detector X-ray diffractometer with graphite-monochromated Mo Kα radiation ($\lambda = 0.71073$ Å). A single crystal of $[Ir(\mathbf{L1})_2](PF_6)_3$ was mounted on a glass fiber. A hemisphere of data was collected in 10-s frames and ω scans of 0.3 deg/frame. Data reduction was performed with SAINT, which corrects for Lorentz polarization.[10] Absorption corrections were applied using SADABS,[11] and the space group was assigned using XPREP in SAINT (Bruker, 2001). The structure was solved by the direct method.[12] Atoms were refined on F^2 by full-matrix least-squares using the SHELXL-97 program.[12]

Measurements of $[Ir(\mathbf{L1})(bpy)Cl](PF_6)_2$ and $[Ir(\mathbf{L1})(\mathbf{L2})](BPh_4)_2$ were made on a Rigaku AFC7S with graphite monochromated Mo Kα radiation ($\lambda = 0.71069$ Å), and the data were collected and processed using CrystalClear (Rigaku). $[Ir(\mathbf{L1})(bpy)Cl](PF_6)_2$ was crystallized as orange blocks and $[Ir(\mathbf{L1})(\mathbf{L2})](BPh_4)_2$ as brown blocks, both by slow diffusion from diethyl ether into an acetonitrile solution. Crystals of both $[Ir(\mathbf{L1})(bpy)Cl](PF_6)_2$ and $[Ir(\mathbf{L1})(\mathbf{L2})](BPh_4)_2$ were mounted on a glass loop. The data were collected at a temperature of −150 ± 1 °C to a maximum 2θ value of 55.0°. The linear absorption coefficient, μ, for Mo Kα radiation is 35.6 cm^{-1}. An empirical absorption correction was applied, which resulted in transmission factors ranging from 0.63 to 1.00. The structure was solved by heavy-atom Patterson methods[13] and expanded using Fourier techniques.[14] Some non-hydrogen atoms were refined anisotropically, whereas the rest were refined isotropically. The structure was refined by full-matrix least-squares[15] on F^2.

The crystal data and structure refinements for $[Ir(\mathbf{L1})_2](PF_6)_3$, $[Ir(\mathbf{L1})(bpy)Cl](PF_6)_2$, and $[Ir(\mathbf{L1})(\mathbf{L2})](BPh_4)_2$ are summarized in Table 1.

Synthesis. 1,3-Bis(1-methyl-benzimidazol-2-yl)benzene (L2H). This ligand was prepared by a procedure similar to that reported

(8) Murov, S. L.; Carmichael, I.; Hug, G. L. *Handbook of Photochemistry*, 2nd ed.; Marcel Dekker: New York, 1993; p 9.

(9) (a) Kober, E. M.; Casper, J. V.; Lumpkin, R. S.; Meyer, T. J. *J. Phys. Chem.* **1986**, *90*, 3722−3734. (b) Islam, A.; Ikeda, N.; Nozaki, K.; Ohno, T. *J. Photochem. Photobiol. A* **1997**, *106*, 61−66.

(10) (a) *SAINT*, version 6.22; Bruker AXS Inc.: Madison, WI, 2001. (b) *SMART*, version 5.625; Bruker AXS Inc.: Madison, WI 2001.

(11) Sheldrick, G. M. *SADABS*; Universitat Gottingen: Gottingen, Germany, 1996.

(12) Sheldrick, G. M. *SHELXS-97: Program for Crystal Structure Solution*; University of Gottingen: Gottingen, Germany, 1997.

(13) *PATTY*: Beurskens, P. T.; Admiraal, G.; Beurskens, G.; Bosman, W. P.; Garcia-Granda, S.; Gould, R. O.; Smits, J. M. M.; Smykalla, C. *The DIRDIF Program System, Technical Report of the Crystallography Laboratory*; University of Nijmegen: Nijmegen, The Netherlands, 1992.

(14) *DIRDIF99*: Beurskens, P. T.; Admiraal, G.; Beurskens, G.; Bosman, W. P.; de Gelder, R.; Israel, R.; Smits, J. M. M. *The DIRDIF-99 Program System, Technical Report of the Crystallography Laboratory*; University of Nijmegen: Nijmegen, The Netherlands, 1999.

(15) Least-squares function minimized: $\Sigma w(|F_o| - |F_c|)^2$, where w = least-squares weights.

for 1,3-bis(1-ethylbenzimidazol-2-yl)benzene,[16] except *N*-methyl-1,2-phenylenediamine was used as the starting material. Isophthalic acid (3.0 g, 18 mmol) and *N*-methyl-1,2-phenylenediamine (4.4 g, 36 mmol) were heated in polyphosphoric acid (75 mL) for 4 h at 100 °C, and then for 4 h at 200 °C. After being cooled to room temperature, the reaction mixture was poured into water (300 mL) and neutralized by 5 M NaOH. The resulting violet precipitate was collected by filtration and washed with water. The solid was dissolved in MeOH by heating. Charcoal was added to the hot solution and filtered. The addition of water to the filtrate caused a white precipitate to appear, which provided an analytically pure product. Yield: 3.1 g (51%). mp 179−180 °C. ^{1}H NMR (DMSO-d_6): δ 8.31 (s, Hphenyl, 1H), 8.05 (d, 2H, $H_{5'}$, J = 7.7 Hz,), 7.80 (t, 1H, $H_{6'}$, J = 7.8 Hz), 7.72 (d, 2H, $H_{1'}$, J = 7.7 Hz), 7.66 (d, 2H, $H_{2'}$, J = 7.7 Hz), 7.33 (t, 2H, $H_{2'}$, J = 7.7 Hz), 7.27 (t, 2H, $H_{3'}$, J = 7.7 Hz), 3.98 (s, 6H, $H_{7'}$). MALDI-TOF−MS: 852.5 ([M − CH_3 − 2H]$^+$ requires 852.2).

[Zn(L1)$_2$](NO$_3$)$_2$. This compound was prepared according to the literature,[17] but the starting material was changed from $Zn(ClO_4)_2$·$6H_2O$ to $Zn(NO_3)_2$·$6H_2O$. ^{1}H NMR (CD_3CN): δ 8.84 (m, 3H, $H_{5,6}$), 7.55 (d, 2H, H_4, J = 7.9 Hz), 7.30 (t, 2H, H_3, J = 7.7 Hz), 7.04 (t, 2H, H_2, J = 7.2 Hz), 6.47 (d, 2H, H_1, J = 7.7 Hz), 4.31 (s, 6H, CH_3−N).

[Ir(ttpy)(bpy)Cl](PF$_6$)$_2$. Ir(ttpy)Cl_3 (0.10 g, 0.16 mmol) and 2,2′-bipyridine (0.025 g, 0.16 mmol) were refluxed in ethylene glycol (30 mL) at 160 °C for 18 h. After the solution was cooled to room temperature and filtered, a solution of NH_4PF_6 (0.4 g, 2.5 mmol) in water (ca. 50 mL) was added to the filtrate. After the solution was filtered and washed with $CHCl_3$ and ether, a yellow precipitate was obtained. Orange-red crystals suitable for X-ray analysis were obtained by the diffusion of ether to an acetonitrile solution. Yield: 0.13 g (82%). Anal. Calcd for $C_{32}H_{25}N_5ClIrP_2F_{12}$·$2CH_3$-CN: C, 40.06; H, 2.89; N, 9.08. Found: C, 39.98; H, 2.94; N, 9.03. ^{1}H NMR (DMSO-d_6): δ 9.76 (d, 1H, $H_{8'}$bpy, J = 5.5 Hz), 9.41 (s, H_5, 2H), 9.15−9.08 (m, 3H, H_4 + $H_{5'}$bpy), 8.89 (d, 1H, $H_{4'}$bpy, J = 8.0 Hz), 8.70 (t, 1H, $H_{6'}$bpy, J = 8.0 Hz), 8.37 (t, 2H, H_3, J = 8.1 Hz), 8.32−8.26 (m, 3H, H_7 + $H_{7'}$bpy), 8.21 (t, 1H, $H_{3'}$bpy, J = 8.0 Hz), 8.02 (d, 1H, $H_{1'}$bpy, J = 5.7 Hz), 7.86 (d, 2H, H_1, J = 5.5 Hz), 7.66 (t, 2H, H_2, J = 6.6 Hz), 7.61 (d, 2H, H_6, J = 8.0 Hz), 7.45 (t, 1H, $H_{2'}$bpy, J = 6.7 Hz, 1H), 2.52 (s, 3H, H_8). ESI−MS m/z: 353.49 (353.57 required for [$C_{32}H_{23}N_5ClIr$]$^{2+}$).

[Ir(L1)$_2$](PF$_6$)$_3$. $IrCl_3$·nH_2O (0.51 g, 1.4 mmol) and **L1** (0.46 g, 1.4 mmol) were refluxed in ethylene glycol (30 mL) at 100 °C for 1 h. After cooling to room temperature and filtration, the residue was washed with $CHCl_3$ and ether. Ir(**L1**)Cl_3 was obtained as a red solid. Ir(**L1**)Cl_3 (0.15 g, 0.23 mmol) and **L1** (0.12 g, 0.34 mmol) were refluxed in ethylene glycol (40 mL) at 220 °C for 1 h. After cooling to room temperature, the solution was filtered, and a solution of NH_4PF_6 (0.8 g, 5.0 mmol) in water (ca. 100 mL) was added to the filtrate. After the solution was filtered and washed with $CHCl_3$ and ether, an orange-red precipitate was obtained. Orange-red crystals suitable for X-ray analysis were obtained by the diffusion of ether to an acetonitrile solution. Yield: 0.17 g (55%). Anal. Calcd for $C_{42}H_{34}N_{10}IrP_3F_{18}$·$2CH_3CN$: C, 39.81; H, 2.91; N, 12.11. Found: C, 40.14; H, 3.10; N, 12.39. ^{1}H NMR (CD_3CN): δ 9.27 (d, 4H, H_5, J = 8.2 Hz), 9.07 (t, 2H, H_6, J = 8.2 Hz), 7.90 (d, 4H, H_4, J = 8.2 Hz), 7.51 (t, 4H, H_3, J = 7.8 Hz), 7.23 (t, 4H, H_2, J = 8.5 Hz), 6.08 (d, 4H, H_1, J = 8.5 Hz), 4.63 (s, H_7, 12H). ESI−MS m/z: 290.43 (290.42 required for [$C_{42}H_{34}N_{10}Ir$]$^{3+}$), 508.20 (508.11 required for [$C_{42}H_{34}N_{10}IrPF_6$]$^{2+}$).

[Ir(L1)(bpy)Cl](PF$_6$)$_2$. Ir(**L1**)Cl_3 (0.05 g, 0.078 mmol) and 2,2′-bipyridine (0.015 g, 0.094 mmol) were refluxed in ethylene glycol (10 mL) for 18 h at 160 °C. After the mixture was cooled to room temperature, the solution was filtered. To the filtrate was added a solution of NH_4PF_6 (0.4 g, 2.5 mmol) in water (ca. 50 mL) to cause the precipitation. The orange-yellow precipitate was collected by filtration and washed with $CHCl_3$. After recrystallization from acetonitrile−ether, orange crystals were obtained. Yield: 0.067 g (85%). Anal. Calcd for $C_{31}H_{25}N_7ClIrP_2F_{12}$·$2CH_3CN$: C, 38.38; H, 2.85; N, 11.51. Found: C, 38.36; H, 3.00; N, 11.14. ^{1}H NMR (CD_3-CN): δ 10.3 (d, 1H, $H_{8'}$bpy, J = 5.8 Hz), 8.79 (d, 1H, $H_{5'}$bpy, J = 8.2 Hz), 8.76−8.70 (m, 3H, H_6 + $H_{6'}$bpy), 8.57 (td, 1H, H_5, J = 8.4, 1.4 Hz), 8.42 (d, 1H, $H_{4'}$bpy, J = 7.7 Hz), 8.27 (ddd, 1H, $H_{7'}$bpy, J = 7.4, 5.9, 1.5 Hz), 7.98 (td, 1H, $H_{3'}$bpy, J = 8.0, 1.4 Hz), 7.76 (d, 2H, H_4, J = 8.5 Hz), 7.69 (d, 1H, $H_{1'}$bpy, J = 5.8 Hz), 7.58 (ddd, 2H, H_3, J = 8.4, 7.4, 1.0 Hz), 7.35 (ddd, 1H, $H_{2'}$-bpy, J = 7.6, 5.9, 1.4 Hz), 7.25 (ddd, 2H, H_2, J = 8.4, 7.3, 0.8 Hz), 6.00 (dd, 2H, H_1, J = 8.5, 0.8 Hz), 4.52 (s, H_7, 6H). ESI−MS m/z: 361.61 (361.57 required for [$C_{31}H_{25}N_7ClIr$]$^{2+}$).

[Ir(L1)(L2)](PF$_6$)$_2$. Ir(**L1**)Cl_3 (0.15 g, 0.24 mmol) and **L2H** (0.12 g, 0.34 mmol) were refluxed in ethylene glycol (35 mL) for 20 h at 210 °C. After the solution was cooled to room temperature, a saturated aqueous solution of NH_4PF_6 was added, and the resulting orange precipitate was filtered off. After recrystallization from acetonitrile−ether, orange crystals were obtained. Yield: 0.11 g (46%). Anal. Calcd for $C_{43}H_{34}N_9IrP_2F_{12}$·$CH_3CN$·$1.5(C_2H_5)_2O$: C, 46.71; H, 3.99; N, 10.68. Found: C, 47.02; H, 3.83; N, 10.65. ^{1}H NMR (DMSO-d_6): δ 9.25 (d, 2H, H_5, J = 8.0 Hz), 8.99 (t, 1H, H_6, J = 8.3 Hz), 8.67 (d, 2H, $H_{5'}$, J = 8.0 Hz), 8.02 (t, 1H, $H_{6'}$, J = 7.7 Hz), 7.80 (d, 2H, H_4, J = 8.6 Hz), 7.69 (d, 2H, $H_{4'}$, J = 8.0 Hz), 7.39 (t, 2H, H_3, J = 7.7 Hz), 7.26 (t, 2H, $H_{3'}$, J = 7.7 Hz), 7.08 (t, 2H, H_2, J = 7.7 Hz), 7.02 (t, 2H, $H_{2'}$, J = 7.7 Hz), 5.96 (d, 2H, H_1, J = 6.9 Hz), 5.93 (d, 2H, $H_{1'}$, J = 6.3 Hz), 4.61 (s, H_7, 6H), 4.46 (s, $H_{7'}$, 6H). ESI−MS m/z: 434.67 (434.63 required for [$C_{43}H_{34}N_9Ir$]$^{2+}$).

For X-ray crystallographic analysis, a BPh_4 salt of [Ir(**L1**)(**L2**)]$^{2+}$ was used instead of a PF_6 salt. [Ir(**L1**)(**L2**)](BPh_4)$_2$ was easily obtained by anion exchange.

[Ir(L1)(L2)](BPh$_4$)$_2$. Anal. Calcd for $C_{91}H_{74}N_9IrB_2$·CH_3CN·$5H_2O$: C, 68.17; H, 5.35; N, 8.55. Found: C, 68.20; H, 5.11; N, 8.30. ^{1}H NMR (CD_3CN): δ 8.93 (d, 2H, H_5, J = 8.6 Hz), 8.77 (t, 1H, H_6, J = 8.3 Hz), 8.50 (d, 2H, $H_{5'}$, J = 8.0 Hz), 7.96 (t, 1H, $H_{6'}$, J = 8.0 Hz), 7.47 (d, 2H, H_4, J = 8.6 Hz), 7.38 (d, 2H, $H_{4'}$, J = 8.6 Hz), 7.35 (t, 2H, H_3, J = 7.4 Hz), 7.28−7.24 (m, 16H, phenyl-B), 7.22 (td, 2H, H_3, J = 7.5, 1.1 Hz), 7.02−6.96 (m, 20H, H_2, $H_{2'}$, phenyl-B), 6.81 (t, 8H, phenyl-B, J = 7.2 Hz), 6.05 (d, 2H, H_1, J = 8.6 Hz), 5.97 (d, 2H, $H_{1'}$, J = 8.6 Hz), 4.41 (s, H_7, 6H), 4.31 (s, $H_{7'}$, 6H). ESI−MS m/z: 434.70 (434.63 required for [$C_{43}H_{34}N_9Ir$]$^{2+}$).

Results and Discussion

Syntheses and Characterizations. The syntheses of Ir(III) complexes with polypyridine ligands require rigorous conditions because of the inertness of the Ir(III) core. Both high temperatures and a long reaction time were also necessary for the syntheses of Ir(III) complexes with the tridentate benzimidazole derivatives. Chromatographic purification for Ir complexes is commonly employed in order to separate a desired complex from undesired side products. For the present Ir complexes, attempts to find the elution

(16) Carina, R. F.; Williams, A. F.; Bernardinelli, G. *Inorg. Chem.* **2001**, *40*, 1826.
(17) Piguet, C.; Bernardinelli, G.; Williams, A. F. *Inorg. Chem.* **1989**, *28*, 2920−2925.

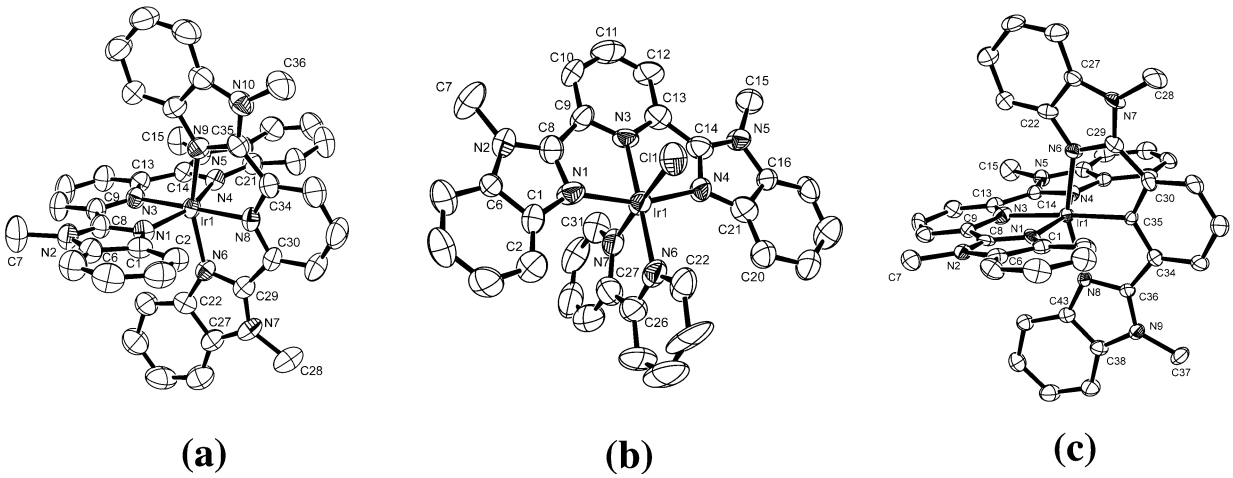

Figure 1. ORTEP diagrams of $[Ir(\mathbf{L1})_2]^{3+}$ (a), $[Ir(\mathbf{L1})(bpy)Cl]^{2+}$ (b), and $[Ir(\mathbf{L1})(\mathbf{L2})]^{2+}$ (c) with 50% probability. H atoms, PF_6^- and BPh_4^- ions, and solvents were omitted for clarity.

Table 2. Selected Bond Lengths, Bond Angles, and Torsion Angles of Ir(III) Complexes

$[Ir(\mathbf{L1})_2](PF_6)_3$	$[Ir(\mathbf{L1})(bpy)Cl](PF_6)_2$	$[Ir(\mathbf{L1})(\mathbf{L2})](BPh_4)_2$
	Bond Lengths (Å)	
Ir(1)−N(1), 2.041(3)	Ir(1)−Cl(1), 2.338(3)	Ir(1)−N(1), 2.068(4)
Ir(1)−N(3), 1.998(3)	Ir(1)−N(1), 2.039(8)	Ir(1)−N(3), 2.037(4)
Ir(1)−N(4), 2.036(3)	Ir(1)−N(3), 1.991(8)	Ir(1)−N(4), 2.049(4)
Ir(1)−N(6), 2.043(3)	Ir(1)−N(4), 2.032(9)	Ir(1)−N(6), 2.060(4)
Ir(1)−N(8), 1.998(3)	Ir(1)−N(6), 2.046(9)	Ir(1)−N(8), 2.056(4)
Ir(1)−N(9), 2.041(3)	Ir(1)−N(7), 2.049(9)	Ir(1)−C(35), 2.018(5)
	Bond Angles (deg)	
N(1)−Ir(1)−N(3), 79.25(12)	N(3)−Ir(1)−N(4), 78.9(3)	N(1)−Ir(1)−C(35), 98.2(2)
N(1)−Ir(1)−N(4), 158.75(11)	N(3)−Ir(1)−N(6), 178.5(4)	N(3)−Ir(1)−C(35), 176.3(2)
N(3)−Ir(1)−N(4), 79.62(12)	N(6)−Ir(1)−N(7), 81.0(4)	N(8)−Ir(1)−C(35), 79.0(2)
N(3)−Ir(1)−N(8), 177.75(12)	N(1)−Ir(1)−N(4), 156.3(2)	
Cl(1)−Ir(1)−N(1), 88.7(3)	N(3)−Ir(1)−N(8), 99.3(2)	
Cl(1)−Ir(1)−N(3), 87.3(2)	N(3)−Ir(1)−N(6), 103.4(2)	
Cl(1)−Ir(1)−N(7), 174.6(3)	N(6)−Ir(1)−N(8), 157.1(2)	
N(1)−Ir(1)−N(3), 80.2(4)	N(6)−Ir(1)−C(35), 78.2(2)	
	Torsion Angles (deg)	
N(1)−C(8)−C(9)−N(3), −6.5(5)	N(1)−C(8)−C(9)−N(3), 0(1)	N(3)−C(13)−C(14)−N(4), −4.1(6)
N(3)−C(13)−C(14)−N(4), 1.1(5)	N(3)−C(13)−C(14)−N(4), −1(1)	C(35)−C(34)−C(36)−N(8), −3.9(7)
N(6)−C(29)−C(30)−N(8), 4.1(5)	N(6)−C(26)−C(27)−N(7), 4(1)	N(6)−C(29)−C(30)−C(35), −1.7(7)
N(8)−C(34)−C(35)−N(9), −2.0(5)	N(1)−C(8)−C(9)−N(3), 2.2(7)	

condition by column chromatography on SiO_2 and alumina have failed so far. However, the synthetic reaction afforded a relatively pure crystalline product, which can be easily purified by recrystallization. The purity of the complexes was carefully checked by elemental analysis, ^{1}H NMR, and ESI−MS spectra. The new Ir(III) complexes were soluble in polar organic solvents such as methanol, acetonitrile, DMSO, and DMF and were scarcely soluble in water. All of the Ir(III) complexes were characterized by ^{1}H NMR, ESI−MS, and elemental analysis. Single crystals suitable for X-ray crystallographic analysis were obtained by recrystallization from acetonitrile−ether.

Perspective views (ORTEP) of the cations $[Ir(\mathbf{L1})_2]^{3+}$, $[Ir(\mathbf{L1})(bpy)Cl]^{2+}$, and $[Ir(\mathbf{L1})(\mathbf{L2})]^{2+}$ are shown in Figure 1a−c, respectively, and selected bond distances and angles are given in Table 2. The coordination geometries of the Ir(III) centers of all three complexes were distorted octahedral. The $Ir-N_{pyridine}$ bond lengths in $[Ir(\mathbf{L1})_2]^{3+}$ and $[Ir(\mathbf{L1})(bpy)Cl]^{2+}$ were 1.98−1.99 Å, shorter than those of $Ir-N_{imidazole}$ (2.02−2.04 Å) as a result of structural constraints of the tridentate ligands. The **L1** ligand of $[Ir(\mathbf{L1})_2]^{3+}$ was not planar, being slightly distorted because of the repulsion between the *N*-methyl groups and the hydrogen of the pyridine moiety. The peripheral $Ir-N_{L1}$ bonds in $[Ir(\mathbf{L1})(bpy)Cl]^{2+}$ were shorter than those for the $Ir-N_{ttpy}$ bonds in $[Ir(ttpy)(bpy)Cl]^{2+}$,[18] and furthermore, the Ir(1)−Cl(1) bond [2.338(3) Å] was almost the same length as the Ir−Cl bond of $[Ir(ttpy)(bpy)Cl]^{2+}$ [2.3343(5) Å]. Concerning the Ir−bpy coordination geometry, the two $Ir-N_{bpy}$ bonds, Ir(1)−N(6) and Ir(1)−N(7), in $[Ir(\mathbf{L1})(bpy)Cl]^{2+}$ were almost the same length [2.046(9) and 2.049(9) Å, respectively], though those for $[Ir(ttpy)(bpy)Cl]^{2+}$ were different [2.0605(16) Å and 2.0354(16) Å, respectively]. The tridentate **L1** ligand and the bipyridine ligand had tilt conformations. As for $[Ir(\mathbf{L1})(\mathbf{L2})]^{2+}$, Ir(1)−C(10) was 2.018(5) Å, much shorter than the Ir−C bonds in the Ir−ppy complexes,[4i] likely because of the structural constraint of the tridentate **L2** ligand. In contrast, Ir(1)−N(7) was 2.037(4) Å, longer than the $Ir-N_{pyridine}$ bond in $[Ir(\mathbf{L1})_2]^{3+}$ [1.998(3) Å]. The elongation of the $Ir-N_{pyridine}$ bond was induced by a trans effect of the

(18) Yutaka, T.; Obara, S.; Haga, M.; Yokoyama, Y.; Sakai, K. Manuscript in preparation.

Table 3. Electrochemical Data[a] for the Ir(III) Complexes

complex	$E^{0'}_{ox}$/V	$E^{0'}_{red}$/V
$[Ir(ttpy)_2]^{3+}$ [b]	>1.7	−1.19,[c] −1.33[c]
$[Ir(L1)_2]^{3+}$	(1.65)[d]	−1.12,[e] −1.34[c]
$[Ir(ttpy)(bpy)Cl]^{2+}$	>1.7	−1.24,[e] −1.49,[c] −1.81[f]
$[Ir(L1)(bpy)Cl]^{2+}$	(1.64)[d]	−1.27,[e] −1.59,[c] −1.77[f]
$[Ir(L1)(L2)]^{2+}$	1.18[f]	−1.44,[e] −1.98[c]

[a] Redox potentials are denoted vs F_c/F_c^+ in 0.1 M Bu_4NBF_4−acetonitrile. [b] In DMF. [c] Irreversible. [d] Measured by differential pulse voltammetry. [e] Quasi-reversible. [f] Reversible.

carbon donors.[4g] Both the **L1** and **L2** ligands were slightly distorted from a coplanar geometry.

Electrochemistry. The redox potentials of the Ir(III) complexes were determined from cyclic voltammograms and are summarized in Table 3. Although no oxidation waves were clearly observed for either $[Ir(ttpy)_2]^{3+}$ or $[Ir(ttpy)(bpy)Cl]^{2+}$ complexes within the available potential window (∼1.7 V), the oxidation waves were observed for $[Ir(\mathbf{L1})_2]^{3+}$ and $[Ir(\mathbf{L1})(bpy)Cl]^{2+}$ around 1.65 V, near the limit of the potential window, by differential pulse voltammetry. These results indicate that the oxidation potentials of the Ir−ttpy complexes are higher than those of the Ir−**L1** complexes. Similar behaviors were also observed for Ru(II) complexes: the oxidation potentials of $[Ru(ttpy)_2]^{2+}$ were 0.55 V higher than that of $[Ru(\mathbf{L1})_2]^{2+}$.[5a] $[Ir(\mathbf{L1})(\mathbf{L2})]^{2+}$ showed a reversible redox wave for an Ir(III/IV) oxidation process at 1.18 V, lower than that of $[Ir(\mathbf{L1})_2]^{3+}$. Moreover, the similarity in the oxidation potentials between $[Ir(\mathbf{L1})_2]^{3+}$ and $[Ir(\mathbf{L1})(bpy)Cl]^{2+}$ indicates that the σ-donating character of **L1** is comparable to that for (bpy + Cl^-). A comparison of the oxidation potentials indicates that the σ-donating character of these tridentate ligands increases in the order ttpy < **L1** ∼ (bpy + Cl^-) < **L2**.

As for reduction behavior, $[Ir(ttpy)_2]^{3+}$ showed two successive irreversible reductions of the ttpy ligand.[4b] $[Ir(\mathbf{L1})_2]^{3+}$ showed quasi-reversible reduction waves characteristic of **L1** ligands at −1.12 and −1.34 V. The $[Ir(N\wedge N\wedge N)(bpy)Cl]^{2+}$-type complexes showed three one-electron reduction processes at −1.27, −1.59, and −1.77 V, in which the first wave was quasi-reversible, the second wave was irreversible, and the third wave was reversible. The first reduction potentials of $[Ir(N\wedge N\wedge N)_2]^{3+}$ were slightly more positive than that of $[Ir(bpy)_3]^{3+}$ (−1.26V).[19] These findings and the similarity in the first reduction potentials between $[Ir(N\wedge N\wedge N)_2]^{3+}$ and $[Ir(N\wedge N\wedge N)(bpy)Cl]^{2+}$ indicate that the first reduction occurs on the tridentate ligand, followed by reduction of the bpy. The slight negative shift in the reduction potentials of $[Ir(N\wedge N\wedge N)(bpy)Cl]^{2+}$ compared to those in $[Ir(N\wedge N\wedge N)_2]^{3+}$ is probably due to the electrostatic effect of the Cl anion. The first reduction potential of $[Ir(\mathbf{L1})(\mathbf{L2})]^{2+}$ was shifted in a negative direction compared to those of the other Ir−**L1** complexes because of the strong σ-donating character of **L2**.

UV−vis Absorption Spectra. The UV−vis absorption spectral data of the Ir(III) complexes are listed in Table 4, and the absorption spectra of the Ir(III) complexes are shown in Figure 2. In the homoleptic Ir(III) complexes, a ligand $\pi-\pi^*$ transition appeared at λ < 320 nm for ttpy and at λ < 378 nm for **L1**. The ligand $\pi-\pi^*$ transition in $[Ru(\mathbf{L1})_2]^{2+}$ has been reported to appear at 313 and 357 nm.[5a] When the central metal ion was changed from Ru(II) to Ir(III), the ligand $\pi-\pi^*$ transition was shifted (∼5 nm) to a longer wavelength. Although ligand $\pi-\pi^*$ transitions often overlap in mixed-ligand complexes, the $\pi-\pi^*$ transition bands for bpy and **L1** in $[Ir(\mathbf{L1})(bpy)Cl]^{2+}$ were found to be well-resolved at around 315 and 354 nm, respectively. In addition to ligand $\pi-\pi^*$ transitions, several weak absorption bands were observed in a longer wavelength region (>400 nm) for $[Ir(\mathbf{L1})_2]^{3+}$ that were not observed for $[Zn(\mathbf{L1})_2]^{2+}$. Similar weak bands were also observed for the other Ir(III) complexes. As for $[Ir(ttpy)_2]^{3+}$, the absorption band at 373 nm exhibited a weak tail to ca. 430 nm. These absorption bands originated from transitions involving dπ orbitals, probably a metal-to-ligand charge transfer (MLCT) transition band that has been observed for analogous Ir(III) complexes.[4] This assignment is supported by findings indicating that the order of the lowest transition energies of the bands, $[Ir(ttpy)_2]^{3+}$ (22×10^3 cm^{-1}) > $[Ir(\mathbf{L1})_2]^{3+}$ (19.4×10^3 cm^{-1}) > $[Ir(\mathbf{L1})(\mathbf{L2})]^{2+}$ (18.8×10^3 cm^{-1}), is correlated with the lowest CT transition energies, calculated as the difference between the first oxidation and the first reduction potentials of each complex: $[Ir(ttpy)_2]^{3+}$ (>23×10^3 cm^{-1}) > $[Ir(\mathbf{L1})_2]^{3+}$ (22.3×10^3 cm^{-1}) > $[Ir(\mathbf{L1})(\mathbf{L2})]^{2+}$ (21.1×10^3 cm^{-1}).

Table 4. Absorption Spectral Data of the Ir(III) Complexes in MeCN at Room Temperature

complex	λ_{abs}/nm (ϵ/M^{-1} cm^{-1})
$[Ir(ttpy)_2]^{3+}$	278 (45 900), 305 (46 200), 321 (43 000), 347 (36 800), 373 (29 000), 452 sh (200)
$[Ir(L1)_2]^{3+}$	312 (31 900), 362 (31 400), 378 (32 800), 439 sh (2570), 515 sh (160)
$[Ir(ttpy)(bpy)Cl]^{2+}$	271 (31 900), 315 (35 300), 350 sh (14 500), 380 sh (6100), 440 sh (1000)
$[Ir(L1)(bpy)Cl]^{2+}$	311 (34 900), 354 (24 100), 420 sh (2700), 452 sh (1300)
$[Ir(L1)(L2)]^{2+}$	296 (40 000), 306 (36 800), 364 (34 400), 474 sh (680), 531 sh (160)
$[Zn(L1)_2]^{2+}$	307 (38 900), 352 (33 400)

Emission Spectra. An acetonitrile solution of $[Ir(\mathbf{L1})_2]^{3+}$ showed a yellow emission at around 550 nm at room temperature, and $[Ir(\mathbf{L1})(\mathbf{L2})]^{2+}$ exhibited an orange emission at 593 nm with a structureless spectrum, as shown in Figure 3. $[Ir(ttpy)(bpy)Cl]^{2+}$ and $[Ir(\mathbf{L1})(bpy)Cl]^{2+}$ in acetonitrile solutions at room temperature produced green and yellow emissions at around 509 and 547 nm, respectively (Figure 4). The emission maximum of $[Ir(ttpy)(bpy)Cl]^{2+}$ was approximately 40 nm blue-shifted compared with those of $[Ir(\mathbf{L1})(bpy)Cl]^{2+}$. In a glass matrix at 77 K, the emission spectra of all the Ir(III) complexes exhibited vibrational progressions with a separation of ca. 1400 cm^{-1}. An acetonitrile solution of $[Zn(\mathbf{L1})_2]^{2+}$ at room temperature exhibited a broad fluorescence with a peak around 400 nm. In a glass matrix, in addition to the fluorescence, a long-lived emission with a well-resolved vibrational structure (1443 cm^{-1}) was observed (Figure 5, dotted line). The emission spectral data of the complexes are summarized in

(19) Bolinger, C. M.; Story, N.; Sullivan, B. P.; Meyer, T. J. *Inorg. Chem.* **1988**, *27*, 4582−4587.

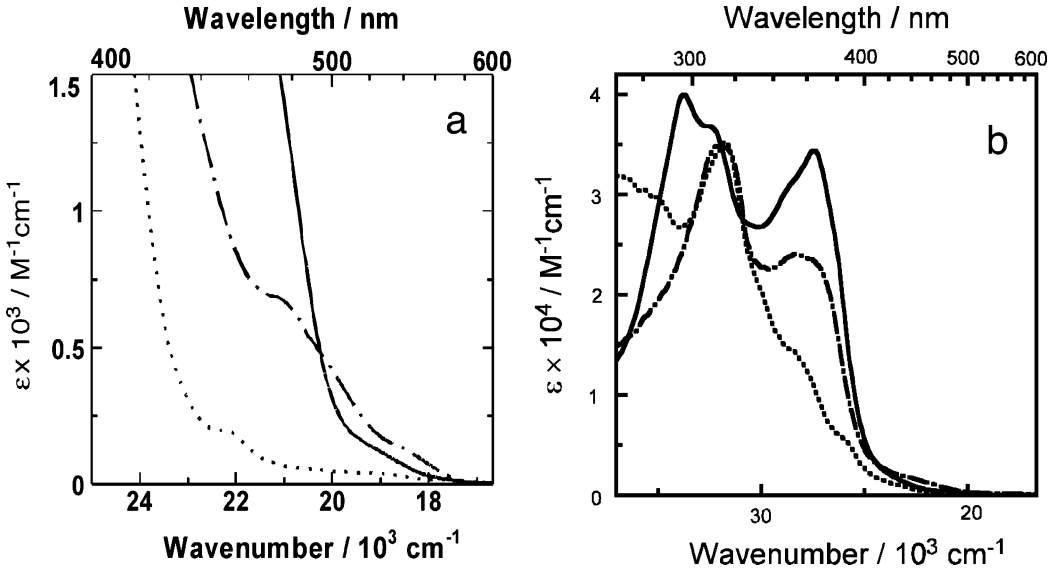

Figure 2. (a) UV−vis spectra of $[Ir(\mathbf{L1})_2]^{3+}$ (solid line), $[Ir(\mathbf{L1})(\mathbf{L2})]^{2+}$ (dashed line), and $[Ir(ttpy)_2]^{2+}$ (dotted line) in MeCN. (b) UV−vis spectra of $[Ir(\mathbf{L1})(\mathbf{L2})]^{2+}$ (solid line), $[Ir(\mathbf{L1})(bpy)Cl]^{2+}$ (dashed line), and $[Ir(ttpy)(bpy)Cl]^{2+}$ (dotted line) in MeCN.

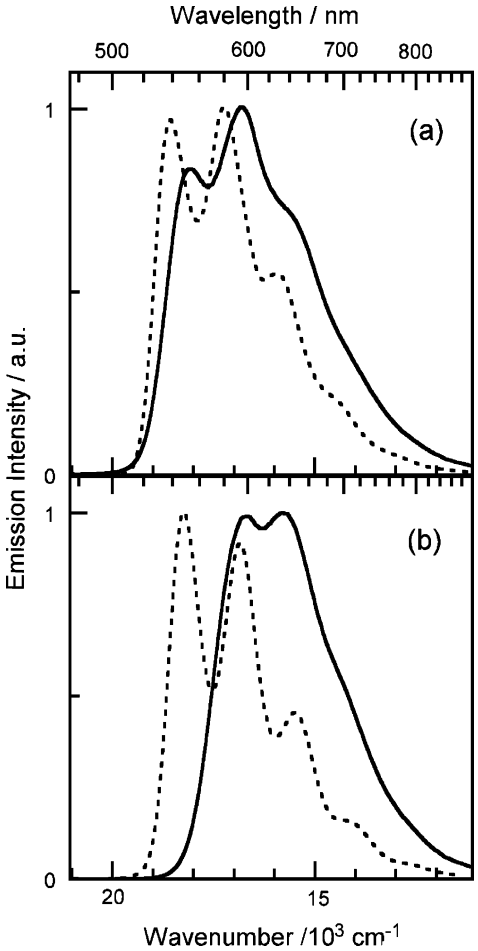

Figure 3. Emission spectra of $[Ir(\mathbf{L1})_2]^{3+}$ (a) and $[Ir(\mathbf{L1})(\mathbf{L2})]^{2+}$ (b). Solid lines are at room temperature (in MeCN), and dotted lines are at 77 K (in DMF−MeOH−EtOH [1:5:5(v/v)].

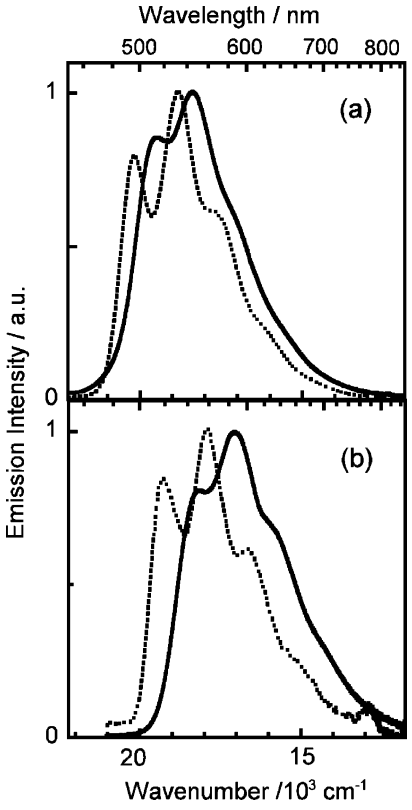

Figure 4. Emission spectra of $[Ir(ttpy)(bpy)Cl]^{2+}$ (a) and $[Ir(\mathbf{L1})(bpy)Cl]^{2+}$ (b). Solid lines are at room temperature (in MeCN), and dotted lines are at 77 K (in DMF−MeOH−EtOH [1:5:5(v/v)].

Table 5. The 0−0 energies for the phosphorescence states were obtained as the highest energy peak in the emission spectra at 77 K. The order of the 0−0 energies, $[Ir(ttpy)_2]^{3+}$ (20.5×10^3 cm^{-1}) > $[Ir(ttpy)(bpy)Cl]^{2+}$ (20.2×10^3 cm^{-1}) > $[Ir(\mathbf{L1})(bpy)Cl]^{2+}$ (19.3×10^3 cm^{-1}) > $[Ir(\mathbf{L1})_2]^{3+}$ (18.5×10^3 cm^{-1}) > $[Ir(\mathbf{L1})(\mathbf{L2})]^{2+}$ (18.3×10^3 cm^{-1}), was in line with that of the lowest transition energies in the absorption spectra.

The emission of Ir(III) diimine complexes has been assigned to phosphorescence from intraligand ^{3}LC or $^3(\pi-\pi^*)$ states.[20] For the $Ir(ppy)_3$ complex, a strong σ-donor ability of ppy decreases the energy level of ^{3}MLCT and

(20) Krausz, E.; Higgins, J.; Riesen, H. *Inorg. Chem.* **1993**, *32*, 4053−4056.

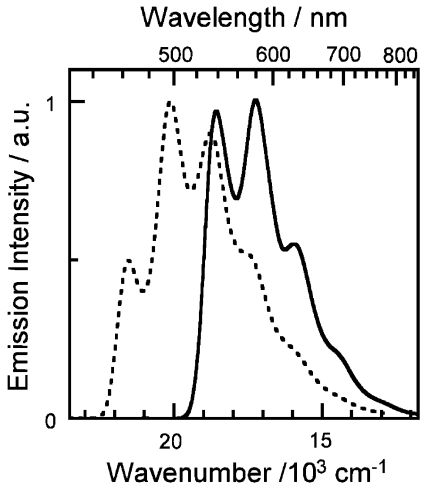

Figure 5. Emission spectra of $[Ir(\mathbf{L1})_2]^{3+}$ (solid line) and $[Zn(\mathbf{L1})_2]^{2+}$ (dotted line) at 77 K in DMF−MeOH−EtOH [1:5:5 (v/v)].

thereby increases the contribution of ^{3}MLCT to the lowest triplet state.[4f,21] Analysis of the 0−0 energies and patterns of the progressions in the emission spectra provide information regarding the characterization of the origins of the emissions. The emission observed for $[Zn(\mathbf{L1})_2]^{2+}$ at 77 K is assigned to an intraligand ^{3}LC or $^3(\pi-\pi^*)$ of **L1** from the analogy of Zn(II) diimine complexes,[22] for which the energy was 21.6×10^3 cm^{-1}. Therefore, the 0−0 energy for $[Ir(\mathbf{L1})_2]^{3+}$ is 3.1×10^3 cm^{-1} lower than the ^{3}LC of **L1**. Similarly, the 0−0 energy for $[Ir(ttpy)_2]^{3+}$ is lower by approximately 2.3×10^3 cm^{-1} than the ^{3}LC of ttpy, which is estimated to be ca. 22.8×10^3 cm^{-1} from the emission spectrum of $[Zn(ttpy)_2]^{2+}$ at 77 K.[4b] The configurational mixing between the ^{3}LC and some other states such as ^{3}MLCT or ^{3}ILCT (interligand CT) is responsible for such low-energy shifts of the 0−0 energies compared with those of the ^{3}LC of the ligands. Because the state energies of ^{3}ILCT in homoleptic complexes must be higher than those of ^{3}LC as a result of the weaker electronic interactions between the hole and the electron, the low-energy shift for $[Ir(N\wedge N\wedge N)_2]^{3+}$-type complexes can be ascribed to the admixture of ^{3}MLCT into ^{3}LC. Fundamentally, ^{3}LC is the main component of the emission of both $[Ir(\mathbf{L1})_2]^{3+}$ and $[Ir(ttpy)_2]^{3+}$, and as for $[Ir(ttpy)_2]^{3+}$, it was suggested in ref 4b that the emission was ascribed mainly to ^{3}LC and some contribution of ^{3}MLCT. The larger magnitude of the low-energy shift for $[Ir(\mathbf{L1})_2]^{3+}$ indicates a greater ^{3}MLCT character of the emitting state compared with that of $[Ir(ttpy)_2]^{3+}$.

Emission spectra for cyclometalated transition-metal compounds often exhibit sidebands corresponding to 1300−1500 cm^{-1} intraligand vibrational modes. The *S* factors of the vibrational modes have often been used to examine the origin of emissions. Emission spectra for ^{3}LC show much larger *S* factors because one electron is promoted from a bonding π orbital of the ligand to an antibonding one. Smaller *S* factors for polypyridine complexes of Ru(II) and Pt(II) indicate that the emissions of the complex have a more MLCT character.[23] The reason for the smaller *S* factors in ^{3}MLCT is that the electrons are promoted from nonbonding d orbitals, not the bonding orbitals of the ligands. Also, for XLCT or some ILCTs[4i] where an electron is promoted from an antibonding between the ligand and metal, *S* factors for intraligand vibrational modes are relatively small. The *S* factor obtained by Franck−Condon analysis[24,25] for a ligand-localized vibrational mode of 1370 cm^{-1} in the emission spectrum of $[Ir(\mathbf{L1})_2]^{3+}$ was 1.3, much smaller than $S = 2.5$ for $[Zn(\mathbf{L1})_2]^{2+}$. This smaller *S* factor also supports our assessment that the emission of $[Ir(\mathbf{L1})_2]^{3+}$ originates from a phosphorescent state with ^{3}LC−^{3}MLCT mixed character.

The characterization of the emitting states in mixed-ligand Ir(III) complexes is more complicated because there are many electronic configurations possibly involving the lowest triplet state. For $[Ir(\mathbf{L1})(\mathbf{L2})]^{2+}$, the electronic configurations to be considered are ^{3}LC(**L1**), ^{3}LC(**L2**), ^{3}MLCT, and ^{3}ILCT(**L2** → **L1**). Because the energy of dπ orbitals is increased as a result of the stronger σ-bonding ability of **L2**, the energy of the ^{3}MLCT state becomes lower and mixing between the dπ and pπ orbitals of **L2** is increased. The low *S* factor (1.1) for $[Ir(\mathbf{L1})(\mathbf{L2})]^{2+}$ undoubtedly indicates that there is less distortion of the ligand structures in the excited state, suggesting a smaller contribution of ^{3}LC in the lowest excited state. Moreover, the emission spectrum observed in a fluid solution of $[Ir(\mathbf{L1})(\mathbf{L2})]^{2+}$ shifted remarkably to a lower energy than that in a glass matrix, as shown in Figure 3b. Stabilization of the excited state due to dipolar interactions between the excited-state dipole moment and orientationally polarized solvents is probably responsible for the low-energy shift of the emission spectra in the fluid solvent. Consequently, the lowest CT energy calculated from redox potentials, the smallest *S* factor, and the largest rigidochromic effect reveals that the lowest excited state of $[Ir(\mathbf{L1})(\mathbf{L2})]^{2+}$ has the largest contribution of ^{3}MLCT in the Ir(III) complexes examined here.

For the mixed-ligand $[Ir(N\wedge N\wedge N)(bpy)Cl]^{2+}$-type complexes, a comparison of the reduction potentials of $[Ir(N\wedge N\wedge N)(bpy)Cl]^{2+}$ with those of $[Ir(bpy)_3]^{3+}$[19] suggests that the LUMO is located primarily on the N∧N∧N ligand. In addition, the energy levels of $^3(\pi-\pi^*)$ for N∧N∧N are lower than those for bpy because the 0−0 energies for both

(21) (a) Colombo, M. G.; Brunold, T. C.; Riedener, T.; Guedel, H. U.; Fortsch, M.; Buergi, H.-B. *Inorg. Chem.* **1994**, *33*, 545−550. (b) Hay, P. J. *J. Phys. Chem.* **2002**, *106*, 1634−1641.

(22) (a) Ohno, T.; Kato, S. *Bull. Chem. Soc. Jpn.* **1974**, *47*, 2953−2957. (b) DeArmond, M. K.; Carlin, C. M.; Huang, W. L. *Inorg. Chem.* **1980**, *19*, 62−67. (c) Ikeda, S.; Yamamoto, S.; Azumi, T.; Crosby, G. A. *J. Phys. Chem.* **1992**, *96*, 6593−6597.

(23) (a) Yip, H.-K.; Cheng, L.-K.; Cheung, K.-K.; Che, C.-M. *J. Chem. Soc., Dalton Trans.* **1993**, 2933−2938. (b) Damrauer, N. H.; Boussie, T. R.; Devenney, M.; McCusker, J. K. *J. Am. Chem. Soc.* **1997**, *119*, 8253−8268. (c) Klassen, D. M.; DelPup, R. V. *Inorg. Chem.* **2002**, *41*, 3155−3160. (d) Amini, A.; Harriman, A.; Mayeux, A. *Phys. Chem. Chem. Phys.* **2004**, *6*, 1157−1164. (e) Jude, H.; Bauer, J. A. K.; Connick, W. B. *Inorg. Chem.* **2004**, *43*, 725−733.

(24) The Huang−Rhys factor (*S*) was defined as $\Delta^2/2$, where Δ is the displacement along a normal vibrational coordinate and, thus, indicates a degree of distortion of the excited state, compared with the ground state along the normal vibrational coordinates.

(25) (a) Caspar, J. V.; Westmoreland, T. D.; Allen, G. H.; Bradley, P. G.; Meyer, T. J.; Woodruff, W. H. *J. Am. Chem. Soc.* **1984**, *106*, 3492−3500. (b) Ruseckas, A.; Namdas, E. B.; Theander, M.; Svensson, M.; Yartsev, A.; Zigmantas, D.; Andersson, M. R.; Inganäs, O.; Sundström, V. *J. Photochem. Photobiol. A* **2001**, *144*, 3−12.

Table 5. Emission Maximum (λ_{em}), Lifetimes (τ), Quantum Yields (Φ), Radiative Rate Constants (k_r), Huang−Rhys Factor (S), and Accepting Mode ($\tilde{\nu}$) of the Ir(III) Complexes

	λ_{em}/nm[a]		τ/μs					
complex	295 K[b]	77 K[c]	295 K	77 K	Φ	k_r/s^{-1}	S	$\tilde{\nu}$/cm^{-1}
$[Ir(ttpy)_2]^{3+}$	506	487, 523, 557	9.5[d]	26[d]	0.11[e]	1.2×10^4 [d]	1.4	1340
$[Ir(L1)_2]^{3+}$	550, 592	538, 578, 624	1.0	13	0.037	3.7×10^4	1.3	1347
$[Ir(ttpy)(bpy)Cl]^{2+}$	509, 541	494, 529	1.2	23	0.043	3.8×10^4	1.6	1339
$[Ir(L1)(bpy)Cl]^{2+}$	547, 582	517, 556, 595	5.7	26	0.19	3.3×10^4	1.5	1406
$[Ir(L1)(L2)]^{2+}$	593, 623	546, 592, 643	1.6	11	0.10	6.3×10^4	1.1	1452
$[Zn(L1)_2]^{2+}$	421(fl.)	400 (fl.) 462, 495, 530	*f*	*f*	*f*	*f*	2.5	1443

[a] $\lambda_{ex} = 355$ nm. [b] In MeCN. [c] In DMF/MeOH/EtOH = 1:5:5 (v/v/v). [d] Ref 4b. [e] Calculated from the results in ref 4b. [f] Fluorescent components could not be separated from the phosphorescent components. [g] Obtained by the Franck−Condon analysis for the uncorrected emission spectrum in ref 4b.

$[Zn(\mathbf{L1})_2]^{2+}$ (21.6×10^3 cm^{-1}) and $[Zn(ttpy)_2]^{2+}$ (22.8×10^3 cm^{-1})[4b] are lower than those for $[Zn(bpy)_3]^{2+}$ (23×10^3 cm^{-1}).[22] Therefore, the properties of the lowest excited states of Ir(N∧N∧N)(bpy)Cl were presumed to be dominated by N∧N∧N ligands. The small S factor (1.5) for $[Ir(\mathbf{L1})(bpy)Cl]^{2+}$ indicates that the emission of $[Ir(\mathbf{L1})(bpy)Cl]^{2+}$ originates from a ^{3}LC mixed with other electronic configurations. The emission spectrum of $[Ir(\mathbf{L1})(bpy)Cl]^{2+}$ shows a rigidochromic shift larger than that for $[Ir(\mathbf{L1})_2]^{3+}$ (Figure 4b), indicating that the excited state of $[Ir(\mathbf{L1})(bpy)Cl]^{2+}$ has a contribution of excited states with large dipole moment such as ^{3}ILCT, ^{3}XLCT (Cl → L1), or ^{3}MLCT.

In summary, analysis of the emission spectra indicates that the emissions of Ir(III) complexes can be assigned to phosphorescence from ^{3}LC mixed with ^{3}MLCT or other ^{3}CT states and that the contribution of ^{3}MLCT in the emitting state can be estimated to be highest in $[Ir(\mathbf{L1})(\mathbf{L2})]^{2+}$. As discussed above, the mixing of ^{3}MLCT into ^{3}LC in the Ir(III)−**L1** and Ir(III)−**L2** complexes is induced by the σ-donor ability of the tridentate **L1** and **L2** ligands.

The rate constants of radiative processes (k_r) were calculated from the lifetimes and the quantum yield of emissions of the Ir(III) complexes and are shown in Table 5. The radiative rate constants for the Ir(III)−ttpy complexes were found to be ca. 1×10^4 s^{-1}, whereas those for the Ir−**L1** complexes were ca. 4×10^4 s^{-1}. The highest k_r among those complexes studied here was obtained for $[Ir(\mathbf{L1})(\mathbf{L2})]^{2+}$ (6.3×10^4 s^{-1}), though this value was lower than that of a highly emitting $Ir(ppy)_3$ ($\tau = 2.0$ μs, $\Phi = 0.4$, $k_r = 2 \times 10^5$ s^{-1}).[4f] It is noteworthy that $[Ir(\mathbf{L1})(\mathbf{L2})]^{2+}$, with the highest contribution of ^{3}MLCT in the emitting state, shows the highest radiative rate of phosphorescence. The origin of the phosphorescence in transition-metal complexes is the mixing of singlet states into the lowest triplet state as a result of spin−orbit coupling of d electrons. The transition dipole moments of the singlet states then cause the radiative capability of the lowest triplet state. According to the first-order perturbation theory, the radiative rate constant of phosphorescence can be calculated from transition dipole moments of singlet-state components involving the lowest triplet states using the following expression:[9,2626 !]

$$k_r = \frac{16\pi^3 \times 10^6 \times \tilde{\nu}^3}{3h\epsilon_o}|M_T|^2 \qquad (1)$$

where $\tilde{\nu}$ is the emission energy of the triplet state in wavenumbers, h and ϵ_o are Planck's constant and the vacuum permittivity, respectively, and M_T is the transition dipole moment for the triplet ground state. M_T can be calculated from the following expression:

$$M_T = \sum_n \frac{\langle \Psi_T | H_{SO} | \Psi_{S_n} \rangle}{^3E_T - {}^1E_{S_n}} M_{S_n} \qquad (2)$$

where Ψ and E are eigenfunctions and eigenvalues of the Hamiltonian without spin−orbit coupling (H_{SO}), respectively. M_{S_n} is the transition dipole moment for the nth singlet state ground state. Equations 1 and 2 indicate that the radiative rate of the phosphorescence strongly depends on the spin−orbit integral between the lowest triplet state and singlet states. The spin−orbit integral is approximated by the one-center one-electron integral, and its magnitude increases when both Ψ_T and Ψ_{S_n} involve orbitals of a larger angular momentum belonging to one atom, such as the 5d orbitals of the Ir(III) ion.[9,26] Therefore, the magnitude of the spin−orbit integral between ^{3}MLCT and ^{1}MLCT must be much larger than that between ^{3}LC and ^{1}LC/^{1}MLCT, which rationalizes the observed trend of the radiative rate constants of the Ir(III) complexes examined here.

The lifetimes at 77 K for $[Ir(ttpy)_2]^{3+}$, $[Ir(ttpy)(bpy)Cl]^{2+}$, and $[Ir(\mathbf{L1})(bpy)Cl]^{2+}$ were found to be longer than 20 μs, whereas those for $[Ir(\mathbf{L1})_2]^{3+}$ and $[Ir(\mathbf{L1})(\mathbf{L2})]^{2+}$ were ca. 10 μs. Although the lifetimes seem to increase with increases in the 0−0 energies, as predicted by the so-called energy gap law,[27] this relationship may not play a definitive role, S factors determined using the Franck−Condon analysis are different in these Ir(III) complexes. The extent of the contribution of ^{3}MLCT in the lowest state also affects the lifetimes. As discussed above, when the lowest triplet state has the character of ^{3}MLCT, the spin−orbit coupling of d orbitals allows the mixing of singlet states into the lowest triplet state and, thereby, both radiative and nonradiative transitions, which are formally spin-forbidden. In fact, a good relationship was found between the lifetimes at 77 K and the k_r values at 295 K, except for $[Ir(\mathbf{L1})(bpy)Cl]^{2+}$. As for $[Ir(\mathbf{L1})(bpy)Cl]^{2+}$, we have pointed out the inconsistency in

(26) Abedin Siddique, Z.; Yamamoto, Y.; Ohno, T.; Nozaki, K. *Inorg. Chem.* **2003**, *42*, 6366−6378.
(27) (a) Robinson, G. W.; Frosch, R. P. *J. Chem. Phys.* **1963**, *38*, 1187−1203. (b) Englman, T.; Jortner, J. *Mol. Phys.* **1970**, *18*, 145−164. (c) Freed, K. F.; Jortner, J. *J. Chem. Phys.* **1970**, *52*, 6272−6291. (d) Henry, B. R.; Siebrand, W. In *Organic Molecular Photophysics*; Birks, J. B., Ed.; Wiley: New York, 1973; Vol. 1. (e) Fong, F. K. *Theory of Molecular Relaxation*; Wiley: New York, 1975.

the character of the emitting states from the analysis of the emission spectra: the emitting state should have less ^{3}MLCT character in a glass matrix at 77 K, although it seems to have more CT character in a fluid solution.

Although the Φ value for [Ir(**L1**)(**L2**)]$^{2+}$ with the highest k_r among the Ir(III) complexes studied here was 0.10, the highest Φ value of 0.19 was obtained for [Ir(**L1**)(bpy)Cl]$^{2+}$. The faster nonradiative deactivation rate of [Ir(**L1**)(**L2**)]$^{2+}$ is responsible for the Φ value being smaller than that of [Ir(**L1**)(bpy)Cl]$^{2+}$. The lifetimes at 295 K are roughly correlated with those at 77 K, except for [Ir(ttpy)(bpy)Cl]$^{2+}$. The large temperature dependence of the lifetimes for [Ir(ttpy)(bpy)Cl]$^{2+}$ suggests the presence of additional decay channels with a thermal barrier. Further investigation will be necessary to better our understanding of the deactivation pathways in the Ir(III) complex.

Summary

Novel Ir(III) complexes with tridentate benzimidazole derivatives exhibited emissions from ^{3}LC−^{3}MLCT mixed states in the 500−600 nm region, and their emissions had more ^{3}MLCT character than those of the Ir(III)−terpyridine complexes. The highest emission quantum yield ($\Phi = 0.19$) was obtained for [Ir(**L1**)(bpy)Cl]$^{2+}$. Radiative rate constants of Ir−**L1** complexes, which were calculated from the lifetime and the quantum yield of emission, increased in the order [Ir(**L1**)(bpy)Cl]$^{2+}$ < [Ir(**L1**)$_2$]$^{3+}$ < [Ir(**L1**)(**L2**)]$^{2+}$. It was hypothesized that the enhanced radiative rate constants of [Ir(**L1**)(**L2**)]$^{2+}$ originated from the greater ^{3}MLCT character in the emitting state as a result of the stronger σ-donor ability of **L2** on the basis of electrochemical, UV−vis, and emission spectral data.[4f] The complex with the highest k_r value does not always exhibit the highest Φ value because Φ is determined not only by k_r but also by the nonradiative rate constant (k_{nr}). Although it may be difficult to control the k_{nr} of the complex by molecular design, it will likely increase the emission quantum yield of the complex to increase the k_r value. An investigation of Ir(III) complexes with other coordination environments with regard to this concept is now in progress.

Acknowledgment. K.N. gratefully acknowledges financial support from the Ministry of Education, Science, Sports, and Culture for a Grant-in-Aid for Scientific Research (Grant 14540515). M.H. gratefully acknowledges financial support from the Institute of Science and Engineering at Chuo University and the Ministry of Education, Science, Sports, and Culture for a Grant-in-Aid for Scientific Research (Grants 15310076 and 16074215 "Chemistry of Coordination Space").

Supporting Information Available: Crystallographic data files of [Ir(**L1**)$_2$](PF$_6$)$_3$, [Ir(**L1**)(bpy)Cl](PF$_6$)$_2$, and [Ir(**L1**)(**L2**)](BPh$_4$)$_2$ in CIF format. This material is available free of charge via the Internet at http://pubs.acs.org.

IC048622Z